Surface thermodynamics of silicate compounds: the case of Zn 2 SiO 4 (001) surfaces and thin films

Jacopo Baima, Jacek Goniakowski, Claudine Noguera, Alexey Koltsov, Jean-Michel Mataigne

Journal Name

ARTICLE TYPE

Cite this: DOI: 00.0000/xxxxxxxxxx

Surface thermodynamics of silicate compounds: the case of Zn_2SiO_4 (001) surfaces and thin films

Jacopo Baima, [abc] Jacek Goniakowski,*[ab] Claudine Noguera,[ab] Alexey Koltsov,[c] and Jean-Michel Mataigne[c]

Received Date
Accepted Date

DOI: 00.0000/xxxxxxxxxx

Silicate compounds are ubiquitous in nature and display a vast variety of structures and properties. Thin silicate films may also form under specific conditions at interfaces between metals and silica. In the present study, we focus on zinc silicate and present a thorough density functional theory-based study of polar and non-polar (001) surfaces of various stoichiometry of its tetragonal polymorph t-Zn_2SiO_4. At the non-polar surfaces, the main features are the existence of the chain reconstruction at the ZnO termination, and the presence of unsaturated surface silanols at the SiO_2 termination. Stabilization of polar surfaces is provided by the formation of O_2^{2-} peroxo groups, reduction of the surface or subsurface Si atoms or formation of Zn_2^{2+} groups, depending upon the surface stoichiometry. While the non-polar stoichiometric and ZnO rich terminations are the most stable in a large part of the accessible phase diagram, the SiO_2 termination is less stable due to the absence of siloxane group formation. We show that, while bulk Zn_2SiO_4 is stable with respect to decomposition into the ZnO and SiO_2 oxides, the same is not true for ultra-thin films due to the fundamental difference of silicate and silica surface energies. Preliminary results show that a similar conclusion could be drawn Fe_2SiO_4. This study opens towards a deeper understanding and possible improvement of zinc adhesion at silica surfaces, of crucial industrial importance.

Introduction

Oxides have long since been used in various applications, ranging from thermal or electrical insulating barriers, to electronics, optoelectronics, or catalysis. Technologies continuously attempt to fine-tune their properties by means of nanostructuration or doping. On the one hand, controlled mixing of two oxides has often been considered as a promising way to engineer their properties, such as toughness, band gaps, or surface reactivities. On the other hand, uncontrolled spontaneous formation of ternary or mixed oxides at interfaces between materials may have non-negligible consequences for the properties of the junction and can be used as a lever for an optimization of its performances.

The role of such interface oxides is particularly interesting in the case of contacts between large gap oxides (such as silica or alumina) and late transition metals (such as zinc), where tuning the interface adhesion is a key challenge for the optimization of, e.g., anti-corrosive zinc coatings. Indeed, if galvanic zinc protection of iron-based materials has long proved its efficiency,[1] the oxidation and surface segregation of light strengthening elements (Al, Si, and Mn) in modern advanced high strength steels (AHSS),[2–7] dramatically reduce zinc adhesion.[8,9]

We have recently shown that the most stable stoichiometric silica terminations, which expose surface siloxane rings interact very weakly with a zinc deposit[10]. Breaking these groups enables the formation of Zn-O bonds, enhances the interfacial interaction, and produces an overall more stable zinc/silica interface. However, it requires crossing substantial energy barriers and is not expected to spontaneously occur. In this context surface pre-hydroxylation appears as a promising route towards breaking surface siloxanes and improving the interface adhesion.[11] Aside application of inox buffer layers, as proposed for the similar zinc/alumina interfaces,[12,13] an alternative solution may rely on the formation of a mixed interfacial oxide phase, such as zinc silicate Zn_2SiO_4.[14–16] Such interfacial phase would impact the interactions occurring at the interface and, depending on the thermodynamic conditions, could enhance the adhesion through various pathways. The lower density of silicon at the silicate surface could, e.g., prevent the formation of siloxane rings, while the existing network of Zn-O bonds could naturally propagate towards the zinc deposit, thus allowing a stronger adhesion. A theoretical assessment of the differences between silicate and silica surface characteristics under different thermodynamic conditions could

[a] CNRS, UMR 7588, Institut des Nanosciences de Paris, F-75005 Paris, France. E-mail: jacek.goniakowski@insp.jussieu.fr
[b] Sorbonne Université, Institut des Nanosciences de Paris, UMR 7588, INSP, F-75005 Paris, France.
[c] ArcelorMittal Maizières Research, voie Romaine, F-57280, Maizières lès Metz, France.

thus help defining appropriate process parameters to promote the adhesion of zinc coating on Si-alloyed steel grades.

In this context, the goal of the present study is twofold. First, in absence of existing data, we report a comprehensive mapping of Zn_2SiO_4 surface energetics in a wide range of thermodynamic conditions and discuss the structural and electronic characteristics and relative stability of polar/non-polar and ZnO rich/SiO_2 rich terminations. Furthermore, we identify and discuss the main differences between the silicate and silica surface characteristics and link them to the presence/absence of surface silanol/siloxane groups. Finally, we show that, while bulk Zn_2SiO_4 is stable with respect to decomposition into its ZnO and SiO_2 components, the same is not true for thin films under a critical thickness due to the fundamental difference of silicate and silica surface energies.

The paper is organized as follows. After presenting the details and settings of the computational approach in Sec. 2, in Sec. 3 we discuss bulk Zn_2SiO_4 proprieties in reference to those of silica and zinc oxide. In Sec. 4 we first describe the alternative (polar and non-polar) surface configurations and then summarize their thermodynamic stability as a function of chemical conditions. Section 5 is devoted to a comparative analysis of silicate and silica surface energetics and to a discussion of its consequences for silicate thin film stability, before the conclusion.

Computational methods and settings

All calculations were performed within the Density Functional Theory (DFT) implemented in VASP (Vienna ab initio simulation package).[17,18] The dispersion-corrected GGA (optB86-vdW) exchange-correlation functional,[19–21] known to improve the description of adhesion characteristics, is used in view of future interface studies. We verified that the inclusion of the van der Waals correction results in a surface energy of the stoichiometric termination of Zn_2SiO_4 larger by 0.23 Jm^{-2} with respect to a pure GGA functional. Similar variations are obtained for ZnO (0.21 Jm^{-2}) and SiO2 (0.26 Jm^{-2}). The trends, as well as the analysis of section 5 and conclusions, are therefore unaffected by the choice of the DFT functional. The interaction of valence electrons with ionic cores is described within the projector augmented wave (PAW) method.[22,23] The Kohn-Sham orbitals are developed on a plane-wave basis set with a cutoff energy of 400 eV (or 500 eV for relaxation of lattice parameters) and the self-consistent iterative solution of the electronic Hamiltonian is pursued until energy differences become less than 10^{-6} eV. Atomic charges are estimated with the partition scheme proposed by Bader,[24,25] and atomic configurations are plotted with VESTA.[26]

Bulk calculations While several zinc silicate polymorphs have been reported to form in thin films and at Si/ZnO or SiO_x/ZnO interfaces[14–16], we have focused on the tetragonal t-Zn_2SiO_4 phase, which forms at a pressure of about 25 kbar,[27] and is only slightly less stable than the rhombohedral willemite. It is the second most stable phase of a series of five zinc silicate polymorphs formed when applying pressure to the willemite mineral, and has been already stabilized in the presence of interfacial strain.[14,16] The atomic structure of the t-Zn_2SiO_4 polymorph (also referred to as Zn_2SiO_4-II)[16,27,28] is represented in Figure 1. In bulk calculations the lattice parameters and atomic coordinates were relaxed

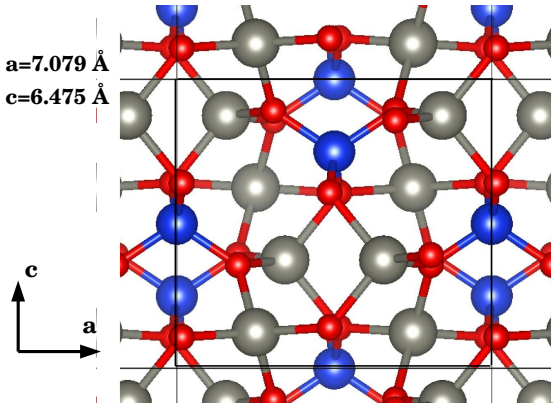

Fig. 1 Bulk structure of t-Zn_2SiO_4. Si, Zn, O atoms are represented by large blue, large grey, and medium red balls, respectively.

until the stress tensor and all forces become smaller than 0.01 eV $Å^{-3}$ and 0.01 eV $Å^{-1}$, respectively. We find that with a Γ-centered 6×6×4 Monkhorst-Pack grid the calculated structural characteristics (lattice parameters, bond lengths, and angles) are converged to within 0.01 Å and 0.1°.

Surface calculations We consider several stoichiometric and non-stoichiometric (001) terminations of t-Zn_2SiO_4, the relative stability of which depends of the values of the oxygen, zinc and silicon chemical potentials μ_O, μ_{Zn} and μ_{Si}, respectively:

$$\sigma = (G^{slab}_{Zn_2SiO_4} - G^{bulk}_{Zn_2SiO_4} - \Delta N_{Si}\mu_{Si} - \Delta N_{Zn}\mu_{Zn} - \Delta N_O\mu_O)/2S \quad (1)$$

where G is the Gibbs free energy of symmetric slab or Zn_2SiO_4 bulk and ΔN_i is the number of excess atoms of specie i with respect to the Zn_2SiO_4 stoichiometry. Since surface terminations are in equilibrium with the underlying bulk silicate, the chemical potentials are related through:

$$g^{bulk}_{Zn_2SiO_4} = 2\mu_{Zn} + 4\mu_O + \mu_{Si} \quad (2)$$

where $g^{bulk}_{Zn_2SiO_4} = G^{bulk}_{Zn_2SiO_4}/N$ is the Gibbs free energy per formula unit, implicitly depending on temperature and pressure. As a consequence, one of the chemical potential in Eq. 1 can always be eliminated by fixing N such that $\Delta N_i = 0$, and the surface energy can be expressed as a function of the other two. In the following, we will use μ_O (which is accessible in the experiment and controls the polarity of the surface) together with either μ_{Zn} or μ_{Si}. We refer μ_O to the total energy of a free oxygen molecule $\Delta\mu_O = \mu_O - \frac{1}{2}E_{O_2}$ and the zinc and silicon chemical potentials to the total energies per atom of the bulk materials $\Delta\mu_{Si,Zn} = \mu_{Si,Zn} - E^{bulk}_{Si,Zn}$. With this choice, $\Delta\mu_i \gtrsim 0$ refers to conditions rich in the specie i (condensation of free oxygen molecules or formation of bulk Si/Zn) and the range of interest for this study is therefore $\Delta\mu_i \leq 0$.

Following standard procedures in *ab initio* thermodynamics, we approximate the free energy difference in Eq. 1 with the difference between the respective total energies at 0 K, obtaining:

$$\sigma(\mu_O,\mu_{Zn}) = (E^{slab}_{Zn_2SiO_4} - E^{bulk}_{Zn_2SiO_4} - \Delta N_{Zn}(E^{bulk}_{Zn} + \Delta\mu_{Zn}) - \Delta N_O(\frac{1}{2}E^{gas}_{O_2} + \Delta\mu_O))/2S \quad (3)$$

and $\sigma(\mu_{Si},\mu_O)$ can be computed analogously.

As to limit the propagation of structural distortions inside the slabs and to improve the convergence with respect to their thickness, we use asymmetric slabs with one bare termination (labelled *B* in the following) and one fully hydroxylated termination (*A* in the following). The latter is chosen as the non-polar SiO_2 rich termination, described in Sec. 4, with 3 dissociated water molecules per surface unit cell.

In this case, the sum of the two surface energies is obtained as:

$$\sigma_B(\mu_{Zn},\mu_O)+\sigma_A(\mu_{Zn},\mu_O)=(E^{a-slab}_{Zn_2SiO_4}-E^{bulk}_{Zn_2SiO_4}$$

$$-\Delta N_{Zn}(E^{bulk}_{Zn}+\Delta\mu_{Zn})-\Delta N_O(\frac{1}{2}E^{gas}_{O_2}+\Delta\mu_O)-3E_{H_2O})/S \qquad (4)$$

with $E^{a-slab}_{Zn_2SiO_4}$ the energy of the asymmetric slab and E_{H_2O} the total energy of a water molecule. Since the evaluation of σ_B requires the knowledge of σ_A, the total energy of a symmetric slab with both terminations equivalently hydroxylated with 3 water molecules each is also calculated:

$$\sigma_A(\mu_{Zn},\mu_O)=(E^{slab}_{Zn_2SiO_4}-E^{bulk}_{Zn_2SiO_4}$$

$$-\Delta N_{Zn}(E^{bulk}_{Zn}+\Delta\mu_{Zn})-\Delta N_O(\frac{1}{2}E^{gas}_{O_2}+\Delta\mu_O)-6E_{H_2O})/2S \qquad (5)$$

Periodic slab replicas are separated by at least 10 Å of vacuum and we use dipole corrections to attenuate the effect of periodic boundary conditions in the direction normal to the slab surfaces.[17,29] The surface structures are obtained by relaxation of bulk cuts. In the cases in which the same surface stoichiometry can be obtained with several different initial geometries, we have relaxed the geometry starting from all initial configurations and retained the lowest energy one. All atoms were relaxed until forces become smaller than 0.01 eV $Å^{-1}$. With such settings 11 atomic layers (either Si or Zn_2O_4) are sufficient to converge the surface energies to within 0.02 Jm^{-2}.

Bulk t-Zn_2SiO_4

Similarly to willemite, bulk t-Zn_2SiO_4 is formed by corner-sharing ZnO_4 and SiO_4 tetrahedra, with SiO_4 surrounded by ZnO_4 and each oxygen ion coordinated to one Si and two Zn atoms. Their structural properties are compared in Table 1. We remind that the experimental structure of t-Zn_2SiO_4 is characterized under pressure p = 70 kbar, and this has to be taken into account when comparing with zero pressure results. Willemite has a larger unit cell with more nonequivalent sites and bonds, but its bond lengths and angles are only little dependent on the local environment. Most importantly, the difference in Si-O and Zn-O bond lengths between the two structures is relatively small ($\leq$1.5%), and smaller than the difference between DFT results obtained with LDA and optB86-vdW exchange-correlation functionals. The O-Zn-O and O-Si-O angles inside the tetrahedra also retain similar values in both structures, with variations within 3%. The only small structural difference originates from different angles between the tetrahedra (Zn-O-Zn and Zn-O-Si), which differ by up to 10% between the two polymorphs. As these are the softest angles in the structure, they tend to bend at surfaces and interfaces even if the connections between tetrahedra are not broken.

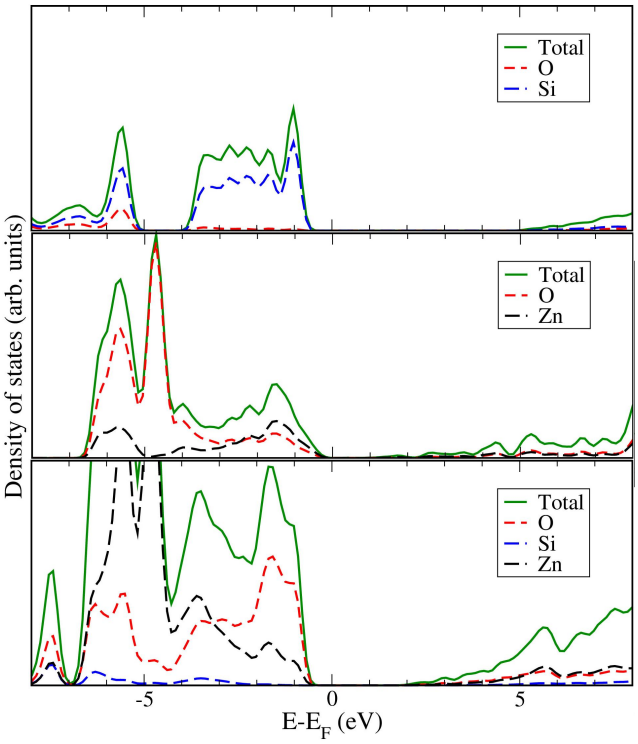

Fig. 2 Local density of states (LDOS) of bulk SiO_2 (top), ZnO (center), and t-Zn_2SiO_4 (bottom) projected on zinc (black), silicon (blue) and oxygen (red) atoms.

Bulk zinc silicate t-Zn_2SiO_4 is 0.2 eV per formula unit more stable than bulk ZnO and SiO_2, compared to 0.28 eV/f.u. measured for willemite.[31] As a consequence, at equilibrium with bulk SiO_2 and Zn (e.g., at the zinc/silica interface), t-Zn_2SiO_4 may form in more oxygen lean conditions, i.e. for $\Delta\mu_O > -3.29$ eV, compared to ZnO, which requires $\Delta\mu_O > -3.19$ eV.

Structural and electronic properties of bulk t-Zn_2SiO_4 are compared to those of bulk SiO_2 and ZnO in Table 2 and Figure 2. From the Bader charges it appears that the ionicity of the Si-O bond in t-Zn_2SiO_4 is similar to that of SiO_2, while the Zn-O bond is more ionic than in ZnO. In the LDOS, both the top of the valence band and the bottom of the conduction band are composed of hybridized Zn-O states, while occupied/unoccupied Si states are found at lower/higher energies, consistently with stronger and more ionic Si-O bonds. The increased ionicity of the Zn-O bond in the silicate accounts for a larger band gap compared to bulk ZnO (2.76 eV wrt 0.77 eV, the numbers which have only a relative significance, due to the known band gap underestimation when using semilocal DFT exchange-correlation functionals).

The bare (001) Zn_2SiO_4 surfaces

As in most oxides, several alternative surface terminations may exist when a bulk is cut along a given orientation. Among them, some are non-polar and others are polar[32,33], and variations in their stoichiometry may further increase the number of configurations to consider. In the following we will successively present the characteristics of the non-polar and polar t-Zn_2SiO_4 (001) sur-

Table 1 Comparison of the computed structural properties [bond lengths (Å), angles (°)] of t-Zn_2SiO_4 with x-ray scattering data obtained under pressure p = 70 kbar and with the willemite structure.

	Si-O	Zn-O	Zn-O-Zn	Zn-O-Si	O-Zn-O	O-Si-O
t-Zn_2SiO_4 (optB86-vdW)	1.64	1.98	116.7	118.0/123.5	101.7/104.4/117.2	108.0/112.4
t-Zn_2SiO_4 (LDA) [16]	1.52	1.93	109.0	118.6/125.0	96/111.2/114.5/120.4	101.5/126.8
t-Zn_2SiO_4 (exp) [28]	1.62	1.98	115.2	117.5/124.8	100.2/106.9/115.5/117.3	107.7/113.2
Willemite (LDA) [16]	1.63/1.64	1.92-1.95	105.6/111.8/112.2	117.1/126.7/128.6/131	105.6-112.2	107.2-111.2
Willemite (exp) [30]	1.63/1.64	1.95/1.98	106.3/109.7/112.3	117.5/120.9/126.0/132.6	103.2-117.0	106.1-110.8

Table 2 Calculated Bader charges Q (e), band gaps E_g (eV), and anion-cation bond lengths d (Å) in bulk t-Zn_2SiO_4, β-cristobalite SiO_2, and wurzite ZnO.

	t-Zn_2SiO_4	SiO_2	ZnO
Q_O (e)	-1.43	-1.59	-1.16
Q_{Zn} (e)	1.29	-	1.16
Q_{Si} (e)	3.12	3.18	-
E_g (eV)	2.76	5.85	0.77
d_{Si-O} (Å)	1.64	1.63	-
d_{Zn-O} (Å)	1.98	-	1.99

faces.

Non-Polar surfaces

Along the (001) direction, the repetitive unit cell is composed of the .../Zn_2O_4/Si/... sequence of atomic layers, with a negligible height difference between the Zn and O atoms (see Fig. 1). These layers have a formal charge of -4 for Zn_2O_4 and +4 for the Si layer, showing that the (001) orientation is polar. To cancel this polarity, the formal charge of the surface layers has to be reduced to ± 2. This is obtained when the number of oxygen atoms in the topmost layer exceeds by one the number of zinc atoms. The three terminations for which this condition is fulfilled are Zn_2O_3/Si/Zn_2O_4/Si/..., ZnO_2/Si/Zn_2O_4/Si/... and O/Si/Zn_2O_4/Si/... In order to label these surfaces in a way that defines their composition as well as their polarity (charge neutrality), we formally assign one oxygen atom from the surface layer to the sub-surface Si. With this choice, the charge neutral (non-polar) terminations given above are labeled Zn_2O_2, ZnO, and SiO_2 (see Fig. 3). Of these three, the ZnO termination is stoichiometric with respect to a dipole-free bulk unit cell, and can be used to build a symmetric stoichiometric ZnO-terminated slab. The Zn_2O_2 and SiO_2 terminations are ZnO rich and SiO_2 rich, respectively.

At the ZnO termination, only weak Zn-O bonds are cut upon surface formation. Moreover, this termination undergoes a significant reconstruction which allows two new Zn-O bonds to be formed. The surface atoms arrange themselves in Zn-O-Si-O chains with a concomitant distortion of bond angles. At variance, if the Zn_2O_2 and SiO_2 terminations have a small total number of broken bonds, strong Si-O bonds are cut upon surface formation. Moreover, at the SiO_2 termination, due to the low density of silicon atoms and the large distance between the surface silanols SiO, no siloxane rings can form contrary to pure silica surfaces [10].

Due to the lower coordination of surface atoms, the electronic structure of the three terminations differs from the bulk one. The reduction of the surface Madelung potential induces a reduction of the band gap of 0.5-0.7 eV and a more covalent character of the surface bonds (smaller Bader charges in Tab. 3). At the SiO_2 termination, the surface states forming the band gap have a slightly enhanced Si-O character (Fig. 4), while in the other two cases the Zn-O character is dominant, similarly to the bulk silicate.

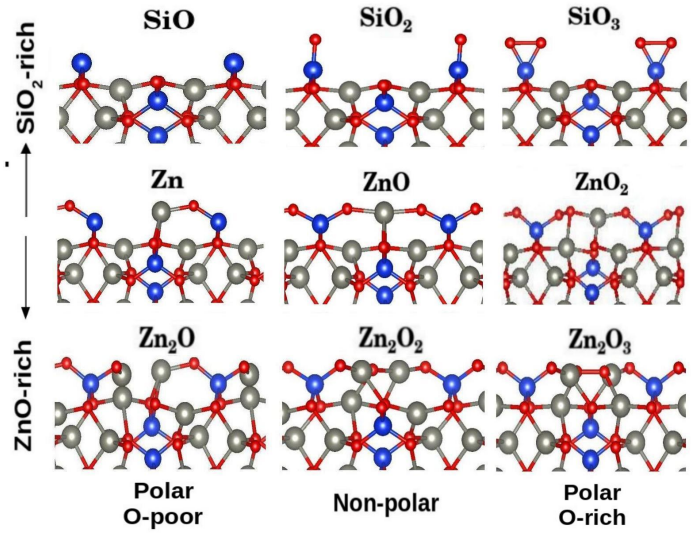

Fig. 3 Atomic structures of the alternative terminations of the (001) surface. Left to right: oxygen lean to oxygen rich. Top to bottom: SiO_2 rich to ZnO rich. In each row, the central configuration is non-polar. Si, Zn, and O atoms are represented by large blue, large grey, and medium red balls, respectively.

Polar surfaces

Six polar terminations can be obtained by addition or subtraction of an oxygen atom to the three non-polar surfaces: the SiO_3, ZnO_2 and Zn_2O_3 oxygen rich terminations, and the SiO, Zn and Zn_2O oxygen lean terminations, which are shown in Fig. 3. Similarly to the non-polar case, SiO_x (x = 1, ..., 3) terminations are SiO_2 rich and Zn_2O_x (x = 1, ..., 3) terminations are ZnO rich.

At all oxygen rich terminations, polarity compensation requires the presence of two holes per surface unit cell. The holes are accommodated via the formation of surface peroxo groups, of O_2^{2-} formal charge. The two oxygen atoms share an equivalent local environment at the SiO_3 and Zn_2O_3 terminations, with either Si-O or Zn-O bonds. In the ZnO_2 case, one oxygen atom is bonded to a surface silicon and the other to two zinc atoms, which results in an asymmetry between their Bader charges. In most cases, nearly pure peroxo states compose the band gap edges (see Fig 4), which reduces its width with respect to the bulk one. How-

Table 3 Calculated Bader charges Q (e) of surface atoms and band gaps E_g (eV) for each surface termination, compared with the corresponding values in bulk zinc silicate.

	SiO	**SiO_2**	SiO_2	Zn	**ZnO**	ZnO_2	Zn_2O	**Zn_2O_2**	Zn_2O_3	Bulk
$Q_{O,peroxo}$ (e)	-		-0.78			-0.58/-0.85			-0.62	
$Q_{O,other}$ (e)	-1.40	-1.35	-1.42	-1.31/-1.38	-1.43/-1.36	-1.42	-1.40	-1.15/-1.41	-1.39	-1.43
Q_{Zn} (e)	1.24	1.26	1.27	1.02	1.30	1.28	0.51/0.85	1.23	1.24	1.29
Q_{Si} (e)	1.65	2.87	3.11	1.97	3.08	3.08	3.09	3.10	3.09	3.12
E_g(eV)	2.18	2.04	1.88	0.1	2.09	1.85	1.75	2.16	2.38	2.76

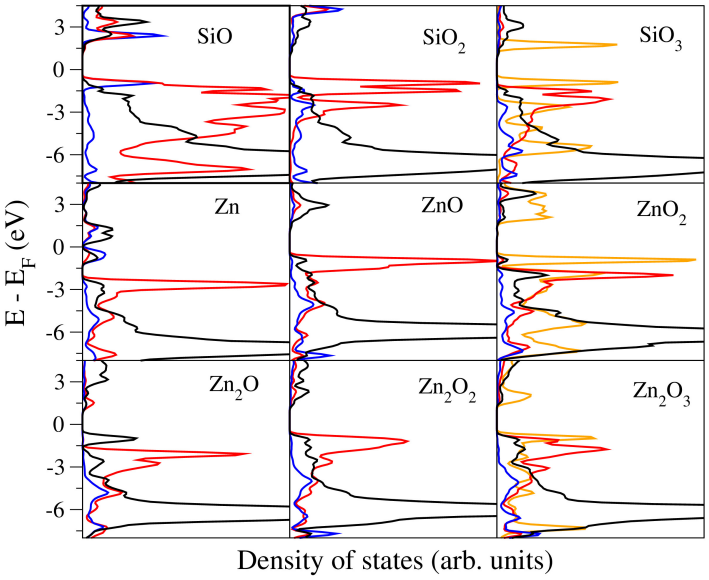

Fig. 4 Local density of states (LDOS) at the (001) surface of t-Zn_2SiO_4 projected on surface zinc (black), silicon (blue), and oxygen atoms (orange for peroxo groups, red for other surface oxygen atoms) at the nine terminations. Left to right: oxygen lean to oxygen rich. Top to bottom: SiO_2 rich to ZnO rich.

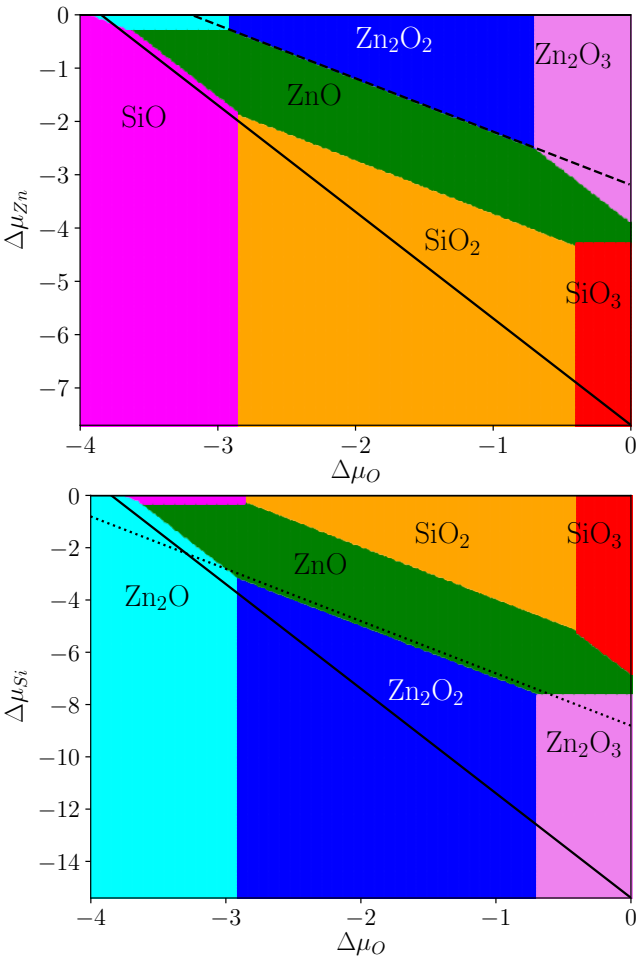

Fig. 5 Surface stability of t-Zn_2SiO_4: most stable surface termination as a function of oxygen and zinc (top) and oxygen and silicon (bottom) chemical potentials. Solid diagonal lines represent $\Delta\mu_{Si}$ =0 (top) and $\Delta\mu_{Zn}$ = 0 (bottom). The dashed (dotted) line in the top (bottom) panel corresponds to the equilibrium with bulk ZnO (SiO_2).

ever, at the Zn_2O_3 termination, due to their strong hybridization with Zn states, the band gap is larger than at the corresponding Zn_2O_2 non-polar termination.

At oxygen lean terminations, two additional electrons per surface cell are needed to cancel the polarity. They are systematically localized at surface cations, but this takes different forms in the three cases. At the SiO termination, the surface silicon atom hosts the excess electrons. Silicon states are shifted towards the gap edges, so that the reduction of E_g is modest. At the Zn termination, the electrons are mostly localized on the sub-surface silicon atoms, with a smaller contribution on the surface zinc atom. This results in a nearly vanishing band gap. Finally, the Zn_2O termination undergoes a significant reconstruction with the formation of a surface Zn_2^{2+} specie. The top of valence bands only involves zinc states, which also results in a large reduction of the band gap.

Surface stability

As stated in Sec. 2, the relative stability of the nine surfaces depends on the values of the excess chemical potentials $\Delta\mu_i$. The top and bottom panels of Fig. 5 show the most stable surface configurations as a function of $(\Delta\mu_O, \Delta\mu_{Zn})$ and $(\Delta\mu_O, \Delta\mu_{Si})$, respectively. They represent two alternative projections of the two

dimensional plane defined by the bulk silicate stability condition, Eq. 2. The solid diagonal lines represents the conditions $\Delta\mu_{Si} = 0$ (upper panel) or $\Delta\mu_{Zn} = 0$ (lower panel). Thus, the upper triangle corresponds in both cases to the area where all $\Delta\mu_i < 0$.

Under most physical conditions, the non-polar surfaces are the most stable, which is consistent with the large energy cost of accommodating the excess charges at the polar terminations. Among them, the Zn_2O_2 one is the most stable in zinc rich conditions, the SiO_2 one in silicon rich conditions, and the stoichiometric ZnO one at intermediate values of the chemical potentials. The existence or absence of surface reconstructions plays an important role. Indeed, the stoichiometric ZnO termination features a significant reconstruction, but the strain on bond lengths and angles prevents it from being stable in a wider range of conditions. Similarly, the absence of siloxane rings at the SiO_2-terminated surface results in its lower stability and prevents it from being more competitive with the ZnO rich terminations.

Polar terminations are only stable under relatively oxygen rich or oxygen lean conditions, Fig. 5. However, contrary to the case of silica where the SiO and SiO_3 terminations are only marginally stable,[10] these terminations can more easily form (for $\Delta\mu_O >$ -0.75 eV or $\Delta\mu_O <$ -2.9 eV) at silicate surfaces, producing potentially more reactive surface configurations. At variance, the Zn and ZnO_2 terminations, obtained by addition/removal of one oxygen to/from the stoichimetric ZnO surface, are not thermodynamically stable under any of considered conditions. As expected, zinc rich conditions favor the Zn_2O termination, oxygen and silicon rich conditions favor the SiO_3 termination, and oxygen and zinc rich environments favor the Zn_2O_3 one.

Discussion

In the following, we first highlight the main differences between the surface energetics of Zn_2SiO_4 and pure SiO_2 and link them to the different nature of the exposed surface species. Then, we discuss the stability of Zn_2SiO_4 in the limit of ultra-thin film.

While Figure 5 gives a comprehensive mapping of most stable silicate surfaces, a complementary picture can be obtained from plots in which one additional condition is imposed to the chemical potentials. Possible choices may involve either an equilibrium with bulk zinc ($\Delta\mu_{Zn} = 0$) or bulk silica ($\Delta\mu_{Si} + 2\Delta\mu_O = E^{bulk}_{SiO_2} - E^{bulk}_{Si} - E_{O_2}$), relevant for zinc silicate formed at the interface between zinc and silica. The energies of all surface terminations can then be plotted as a function of a single chemical potential $\Delta\mu_O$, as shown in Fig. 6.

When a silicate surface is in equilibrium with bulk zinc (top panel of Fig. 6), the most stable termination is always one of the three ZnO rich ones: Zn_2O, Zn_2O_2, or Zn_2O_3. Similarly, when at equilibrium with bulk silica (bottom panel), the most stable termination in a wide range of chemical potential μ_O is the stoichiometric ZnO one, the ZnO rich Zn_2O_2 termination being very close in energy. Under extreme values of the oxygen chemical potential, the stable polar terminations are also ZnO rich. We note that the calculated energies of the stoichiometric ZnO and Zn_2O_2 terminations (1.3 Jm^{-2}, when in equilibrium with bulk ZnO) are hardly larger than that of the most stable stoichiometric wurtzite ZnO $(10\bar{1}0)$ surface (1.1 Jm^{-2}).

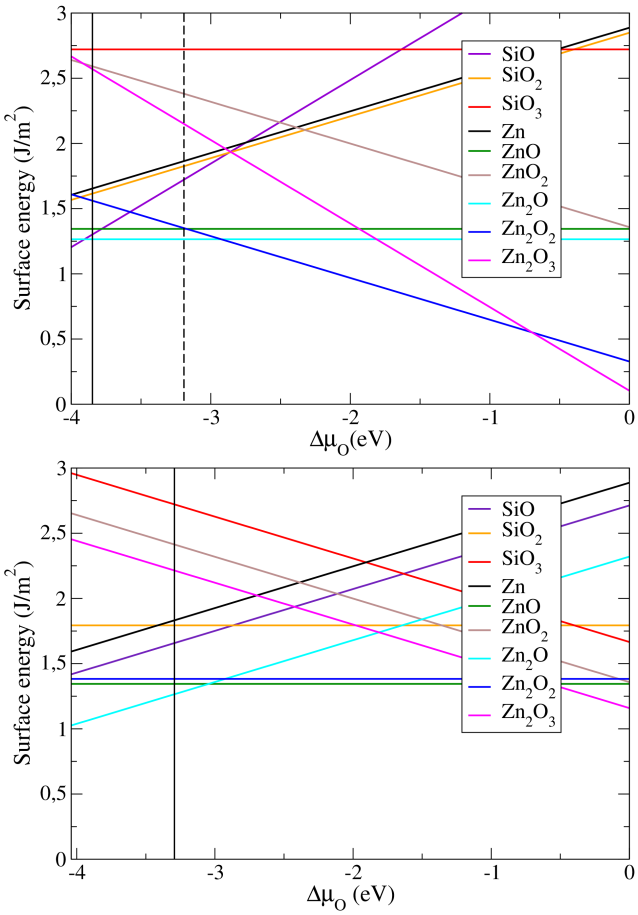

Fig. 6 Calculated surface energies of the different terminations of the t-Zn_2SiO_4 (001) surface as a function of oxygen chemical potential $\Delta\mu_O$, obtained for equilibrium with either bulk zinc (top) or with bulk SiO_2 (bottom). Solid vertical lines represent $\Delta\mu_{Si} = 0$ (top) and $\Delta\mu_{Zn} = 0$ (bottom) and the dashed line represents equilibrium with bulk ZnO (see text).

Conversely, regardless of the precise thermodynamic conditions, the three SiO_2 rich terminations (SiO, SiO_2, and SiO_3) are significantly less stable. Interestingly, in equilibrium with bulk silica, the energy of the stoichiometric silicate SiO_2 termination (1.8 Jm^{-2}) is substantially larger than that of the stoichiometric β-cristobalite (001) SiO_2 termination (1.0 Jm^{-2}). Indeed, in pure silica, the corresponding stability diagram, Fig. 7,[10] shows that the SiO_2 surface energy is greatly reduced upon formation of surface siloxane rings (D_2-SiO_2 termination). However, since such rings cannot form at silicate surfaces because of the lower density of surface Si-O silanol groups, the energy of the silicate SiO_2 termination is rather comparable to that of the much less stable unreconstructed silica surface (SiO_2 termination in Fig. 7) and remains higher than these of the ZnO and Zn_2O_2 terminations.

Beyond the lower stability of SiO_2 rich surfaces, we will show that the absence of silanol polymerization may also produce a thermodynamic bias for the decomposition of silicate nanoobjects (e.g., thin films) into silica and zinc oxide. In the bulk, the mixing energy E^{bulk}_{mix} is estimated from the total energies of

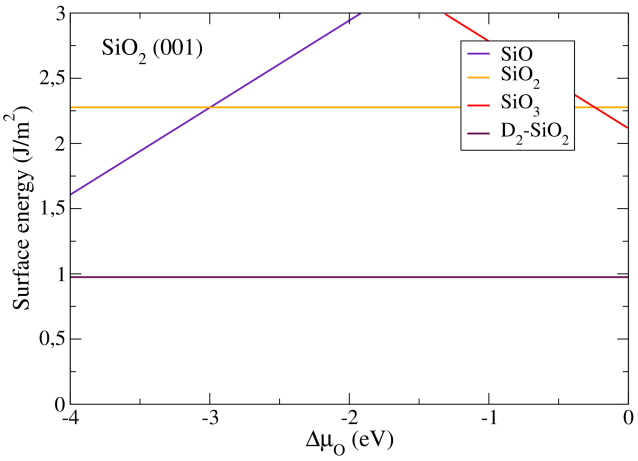

Fig. 7 Calculated surface energies of the different terminations of the SiO_2 (001) surface as a function of oxygen chemical potential $\Delta\mu_O$. The D_2-SiO_2 termination is the reconstructed non-polar termination with two-membered siloxane rings. Adapted from Ref. 10.

bulk Zn_2SiO_4, SiO_2, and ZnO materials as:

$$E^{bulk}_{mix} = E^{bulk}_{Zn_2SiO_4} - E^{bulk}_{SiO_2} - 2E^{bulk}_{ZnO} \quad (6)$$

It is negative, E^{bulk}_{mix} = -0.2 eV/f.u., when t-Zn_2SiO_4 is referred to β-cristobalite SiO_2 and wurtzite ZnO, showing that t-Zn_2SiO_4 is stable with respect to the two constituting oxides. For the most stable silicate structure (willemite), E^{bulk}_{mix} is even more negative and closer to the experimental value of -0.28 eV/f.u..

In analogy to its evaluation in oxide clusters[34], the mixing energy (per formula unit) in thin films E^{film}_{mix} can be derived from the total energy of a silicate slab, referred to SiO_2 and ZnO slabs containing as a whole the same number of ions and exposing the same number of surfaces. This can be obtained by calculating slabs containing n, $2n$, and $4n$ formula units for Zn_2SiO_4, SiO_2, and ZnO respectively, and averaging the binary oxide energies:

$$E^{film,n}_{mix} = [E^{film,n}_{Zn_2SiO_4} - \frac{1}{2}(E^{film,2n}_{SiO_2} + E^{film,4n}_{ZnO})]/n \quad (7)$$

In the explicit DFT calculations of the film mixing energy we have systematically used slabs which expose the smallest surface cell area of the most stable surface, as to minimize their total energies for the given number of formula units. For $n = 4$ (silicate film thickness of about 7 Å) we find a positive E^{film}_{mix} = 1.0 eV/f.u., thus unambiguously showing that at this thickness the silicate film is unstable with respect to decomposition into $(10\bar{1}0)$-oriented ZnO and β-cristobalite SiO_2(001) films.

This result can be rationalized by considering the different surface characteristics of silica and silicate discussed above. Indeed, if the total energy of a film $E^{film,n}$ is approximated as $E^{film,n} \sim nE^{bulk} + 2SE^{surf}$, with S the unit cell surface area and E^{surf} the energy of a semi-infinite surface, the film mixing energy, Eq. 7, reads:

$$E^{film,n}_{mix} \sim E^{bulk}_{mix} + \delta E^{surf}/n \quad (8)$$

It involves the bulk mixing energy E^{bulk}_{mix} and a surface term δE^{surf} which reads:

$$\delta E^{surf} = 2S_{Zn_2SiO_4}E^{surf}_{Zn_2SiO_4} - S_{SiO_2}E^{surf}_{SiO_2} - S_{ZnO}E^{surf}_{ZnO} \quad (9)$$

With the calculated surface energies equal to $E^{surf}_{Zn_2SiO_4}$ =1.34 Jm^{-2}, $E^{surf}_{SiO_2}$ =0.97 Jm^{-2}, and E^{surf}_{ZnO} =1.12 Jm^{-2}, and the corresponding surface areas of $S_{Zn_2SiO_4}$ = 50 Å^2, S_{SiO_2} = 48 Å^2, and S_{ZnO} = 17 Å^2, we obtain a positive surface term δE^{surf} = 4.2 eV and $E^{film,n=4}_{mix}$ = 0.9 eV/f.u., consistent with the above explicit computational estimation.

According to the equation 8, the silicate film is thus unstable with respect to decomposition into the constituting oxide films for thicknesses below $n = -\delta E^{surf}/E^{bulk}_{mix} \sim$ 20 f.u.. The positive value of δE^{surf}, which drives such silicate instability in the limit of small film thickness, reflects the difference between the surface energies of the three materials. To a large extent, it is due to the substantial difference between pure SiO_2 and Zn_2SiO_4 surface energies, driven by the absence of siloxane groups at silicate surfaces.

As to put a broader perspective to these findings, we have attempted a preliminary estimation of analogous decomposition of iron silicate films. To this goal we have considered iron silicate Fe_2SiO_4 in its spinel phase,[35,36] which is structurally similar to the t-Zn_2SiO_4 one and is favored over fayalite under higher pressures. Considering the decomposition of a Fe_2SiO_4 film into pure SiO_2(001), Fe_2O_3(0001), and Fe(110) films, the mixing energy involves the following surface energy term:

$$\delta E^{surf} = 2S_{Fe_2SiO_4}E^{surf}_{Fe_2SiO_4} - \tfrac{2}{3}(S_{SiO_2}E^{surf}_{SiO_2} + S_{Fe_2O_3}E^{surf}_{Fe_2O_3} + S_{Fe}E^{surf}_{Fe}) \quad (10)$$

With the calculated surface energies equal to $E^{surf}_{Fe_2SiO_4}$ = 1.21 Jm^{-2}, $E^{surf}_{Fe_2O_3}$ = 1.52 Jm^{-2}, and E^{surf}_{Fe} =2.12 Jm^{-2}, and surface areas of $S_{Fe_2SiO_4}$ = 33.8 Å^2, $S_{Fe_2O_3}$ = 25.4 Å^2, and S_{Fe} = 5.9 Å^2, we obtain δE^{surf} = 1.0 eV. Although smaller than in the case of Zn_2SiO_4, the positive value of δE^{surf} clearly shows that also in this case the exposed surfaces reduce the stability of a thin silicate film with respect to its constituents. As a reference, the experimental mixing energy of bulk fayalite is equal to -0.2 eV/f.u. only. Interestingly, the decomposition of silicate film may not occur in the case of Mn_2SiO_4, for which the bulk term is much more negative (-0.51 eV/.f.u. with respect to MnO and SiO_2)[31] and the positive surface term is even smaller due to the relatively low MnO(100) surface energy (0.7 Jm^{-2} within DFT-GGA)[37].

Conclusions

We have performed a thorough study of the t-Zn_2SiO_4 bulk and (001) surfaces, using a DFT approach. We have considered all possible surface compositions in a (1×1) unit cell, leading to alternative non-polar and polar terminations. We have analyzed surface electronic and energetic characteristics and have highlighted the existence or absence of surface reconstructions.

At the non-polar surfaces, the low coordination of surface atoms induces little modifications of the electronic structure compared to the bulk silicate. The main features are the existence of

the chain reconstruction at the ZnO termination, and the absence of siloxane groups at the SiO_2 termination. At the polar surfaces, polarity is healed thanks to the formation of O_2^{2-} peroxo groups under oxygen excess, while under oxygen deficiency, the compensating charges are provided either by reduction of the surface or subsurface Si atoms or by the formation of Zn_2^{2+} groups. These processes mainly impact the nature of the band edges and the gap width.

The relative stability of the various surface terminations has been determined as a function of the oxygen, zinc, and/or silicon chemical potentials. We find that the non-polar stoichiometric and ZnO rich terminations are the most stable in a large part of the accessible phase diagram. We assign the relatively low stability of the non-polar SiO_2 termination to the absence of reconstruction of its surface silanols into siloxane rings.

As a first step towards the understanding of zinc silicate formation at the interface between zinc and silica, we have determined the mixing properties of ZnO and SiO_2 to form Zn_2SiO_4 both in the bulk and in thin silicate films. While bulk Zn_2SiO_4 appears stable with respect to decomposition into the two constituting oxides, we find that the same is not true for thin films under a critical thickness. We assign the thin film instability to the fundamental difference between the surface energies in silica and in silicates due to the presence/absence of silanol reconstruction into siloxane rings. Preliminary calculations show that a similar conclusion could be drawn also for the Fe_2SiO_4 silicate.

This study opens the way towards the analysis of formation of interface zinc silicate and its consequences for zinc adhesion at silica surfaces under various thermodynamic conditions, of crucial industrial importance.

Acknowledgments

J. Baima acknowledges a post-doctoral grant from ArcelorMittal Maizières Research. This work was supported by HPC resources from GENCI-IDRIS (Grant 2017-A0010906855).

References

1 A. R. Marder, *Prog. Mater. Sci.*, 2000, **45**, 191–271.
2 H.-T. Jiang, W. Ding, D. Tang and W. Huang, *J. Iron and Steel Research*, 2012, **19**, 29–36.
3 *Advanced high strength sheet steels*, ed. N. Fonstein, Springer Int. Publishing, Switzerland, 1st edn., 2015.
4 B. Hu, H. Luo, F. Yang and H. Dong, *J. Mater. Sci. Technol.*, 2017, **33**, 1457–1464.
5 Q. Tonizzo, A.-F. Gourgues-Lorenzon, M. Maziére, A. Perlade and I. Zuazo, *Mater. Sci. Eng. A*, 2017, **706**, 217–226.
6 J. Emo, P. Maugis and A. Perlade, *Comput. Mater. Sci.*, 2016, **125**, 206–217.
7 W. Wang, M. Li, C. He, X. Wei, D. Wang and H. Dub, *Materials and Design*, 2013, **47**, 510–521.
8 A. Mertens, E. M. Bellhouse and J. R. McDermid, *Materials Science & Engineering A*, 2014, **608**, 249–257.
9 P. Drillet, Z. Zermout, D. Bouleau, J.-M. Mataigne and S. Claessens, *Rev. Metall.-Cah. Inf. Tech.*, 2004, **10**, 831–837.
10 H.-L. T. Le, J. Goniakowski, C. Noguera, A. Koltsov and J.-M. Mataigne, *Physical Chemistry Chemical Physics*, 2018, **20**, 6254–6263.
11 H.-L. T. Le, J. Goniakowski, C. Noguera, A. Koltsov and J.-M. Mataigne, *Physical Chemistry Chemical Physics*, 2018, **20**, 15581–15588.
12 H.-L. T. Le, J. Goniakowski, C. Noguera, A. Koltsov and J.-M. Mataigne, *J. Phys. Chem. C*, 2017, **121**, 25143–25151.
13 H.-L. T. Le, J. Goniakowski, C. Noguera, A. Koltsov and J.-M. Mataigne, *J. Phys. Chem. C*, 2016, **120**, 9836–9844.
14 X. Xu, P. Wang, Z. Qi, H. Ming, J. Xu, H. Liu, C. Shi, G. Lu and W. Ge, *Journal of Physics: Condensed Matter*, 2003, **15**, L607.
15 H. He, Y. Wang and Y. Zou, *Journal of Physics D: Applied Physics*, 2003, **36**, 2972.
16 S. Z. Karazhanov, P. Ravindran, P. Vajeeston, A. G. Ulyashin, H. Fjellvåg and B. G. Svensson, *Journal of Physics: Condensed Matter*, 2009, **21**, 485801.
17 G. Kresse and J. Furthmuller, *Phys. Rev. B*, 1996, **54**, 11169–11186.
18 G. Kresse and J. Hafner, *Phys. Rev. B*, 1993, **47**, 558–561.
19 M. Dion, H. Rydberg, E. Schroder, D. C. Langreth and B. I. Lundqvist, *Phys. Rev. Lett.*, 2004, **92**, 246401.
20 J. Klimes, D. R. Bowler and A. Michaelides, *J. Phys.: Cond. Matt.*, 2010, **22**, 022201.
21 J. Klimes, D. R. Bowler and A. Michaelides, *Phys. Rev. B*, 2011, **83**, 195131.
22 P. E. Blöchl, *Phys. Rev. B*, 1994, **50**, 17953–17979.
23 G. Kresse and J. Joubert, *Phys. Rev. B*, 1999, **59**, 1758–1775.
24 R. F. W. Bader, *Chem. Rev.*, 1991, **91**, 893–928.
25 G. Henkelman, A. Arnaldsson and H. Jonsson, *Comput. Mater. Sci.*, 2006, **36**, 354–360.
26 K. Momma and F. Izumi, *J. Appl. Crystallogr.*, 2011, **41**, 1272–1276.
27 Y. Syono, S.-I. Akimoto and Y. Matsui, *Journal of Solid State Chemistry*, 1971, **3**, 369–380.
28 F. Marumo and Y. Syono, *Acta Crystallographica Section B*, **27**, 1868–1870.
29 J. Neugebauer and M. Scheffler, *Phys. Rev. B*, 1992, **46**, 16067–16080.
30 K.-H. Klaska, J. Eck and D. Pohl, *Acta Crystallographica Section B: Structural Crystallography and Crystal Chemistry*, 1978, **34**, 3324–3325.
31 M. W. C. Jr., *J. Phys. Chem. Ref. Data*, 1998, **Monograph 9**, 1–1951.
32 C. Noguera, *Journal of Physics: Condensed Matter*, 2000, **12**, R367.
33 J. Goniakowski, F. Finocchi and C. Noguera, *Rep. Prog. Phys.*, 2008, **71**, 016501.
34 A. Cuko, M. Calatayud and S. T. Bromley, *Nanoscale*, 2018, **10**, 832–842.
35 A. Ringwood, *Geochimica et Cosmochimica Acta*, 1958, **15**, 18–29.
36 M. Derzsi, P. Piekarz, P. T. Jochym, J. Łażewski, M. Sternik, A. M. Oleś and K. Parlinski, *Physical Review B*, 2009, **79**,

205105.
37 V. Bayer, C. Franchini and R. Podloucky, *Phys. Rev. B*, 2007, **75**, 035404.